Theoretical Study on the Reaction Path and Variational Rate Constant of the Reaction HNCO + NH → NCO + NH_2

Zhen-Feng Xu and Jia-Zhong Sun*

Institute of Theoretical Chemistry, Jilin University, Changchun 130023, People's Republic of China

Received: September 10, 1997; In Final Form: November 18, 1997

The hydrogen abstraction reaction HNCO + NH → NCO+NH_2 has been studied using ab initio molecular orbital theory. The geometries of the reactants, hydrogen-bonded complex, transition state, and products have been optimized at the UMP2/6-311G** level of theory. The forward and reverse reaction potential barriers calculated accurately at the UQCISD(T)/6-311G** level of theory are 25.80 and 2.39 kcal/mol, respectively, and the heat of reaction is 20.32 kcal/mol. The minimum-energy path was calculated by the intrinsic reaction coordinate theory (IRC) at the UMP2/6-311G** level with a gradient step size of 0.05 $(amu)^{1/2}$ a_0. The changes of the geometries and normal-mode vibrational frequencies along the IRC were discussed. The energy profile along the IRC was refined by the UMP4/6-311G** and UQCISD(T)/6-311G** single-point energy calculations. The forward and the reverse reaction rate constants for the temperature range 1000−3000 K were obtained by the variational transition-state theory. The theoretical rate constants of the forward reaction are 2.7, 10.2, and 20.5 times the experimental rate constants at the temperatures 1000, 2000, and 3000 K, respectively. The reverse reaction rate constants are at least an order of magnitude greater than the forward reaction rate constants.

Introduction

Isocyanic acid (HNCO) has been assumed to play an important role in the $RAPRENO_x$ process leading to nitric oxide (NO) removal at high temperature.[1] The initiation steps of the $RAPRENO_x$ process comprise the two reactions

$$HNCO \rightarrow NH + CO \qquad NH + NO \rightarrow H + N_2O$$

and the next steps are a series of radical reactions. Hydrogen abstraction reaction of isocyanic acid and imidogen radical (NH)

$$HNCO + NH \rightarrow NCO + NH_2$$

is one of these reactions and was applied to model the experimental data of the $RAPRENO_x$ mechanism.[2] In 1991, in a shock tube kinetic study of the H + HNCO reaction over the temperature range 2340−3270 K, Mertens et al.[3] presented a rate constant expression, $2.0 \times 10^{13} \exp(-12\,000/T)$ cm^3 mol^{-1} s^{-1}, for the hydrogen abstraction reaction of HNCO + NH. To our best knowledge, this reaction has not been theoretically investigated yet. Thereby, it is necessary to use ab initio molecular orbital theory and direct dynamical method for exploring the properties of the hydrogen abstraction process over the larger range of temperature 1000−3000 K.

In second section of this paper, theoretical methods and calculation details are briefly summarized. The third section represents the location of the stationary points and minimum-energy path (MEP). The information about the potential energy, the goemetric changes, and the generalized normal-mode vibrational frequencies along the intrinsic reaction coordinate (IRC) are discussed. At the end of the third section, the theoretical rate constants using the improved potential energy curve are presented and compared with the experimental values.

Calculational Methods

In this work, standard ab initio molecular orbital calculations were carried out with the GAUSSIAN 92 program[4] for the stationary points on the reaction path of the title reaction. The geometries of all the stationary points were optimized by using the spin-unrestricted second-order Møller−Plesset perturbation theory with the 6-311G** basis set (UMP2/6-311G**).[5] Furthermore, the single-point energy calculations in the fourth-order Møller−Plesset perturbation theory (UMP4/6-311G**)[6] and the quadratic configuration interaction theory including single and double substitutions with a triples contribution (UQCISD(T)/6-311G**)[7] were performed at the UMP2/6-311G** optimized geometries.

The minimum-energy path (MEP) was calculated by the intrinsic reaction coordinate theory (IRC)[8−10] at the UMP2/6-311G** level with a gradient step size of 0.05 $(amu)^{1/2}$ a_0. At some points along the IRC, we computed the matrix of force constants, the harmonic vibrational frequencies, and the corresponding normal-mode vectors for the $3N-7$ degrees of freedom transverse to the reaction path. Because the shape of the potential energy curve is an important factor affecting the rate constant, several points near the TS along the UMP2 potential profile were refined at the UMP4 and UQCISD(T) levels with the same basis set.

The canonical variational transition state theory (CVT) rate constant[11−15] can be obtained by variationally minimizing the generalized transition-state theory rate constant $k^{GT}(T,s)$ with respect to the dividing surface at s, that is,

$$k^{CVT}(T) = \min_s k^{GT}(T,s)$$

where

$$k^{GT}(T,s) = \frac{\sigma Q^{GT}(t,s)}{\beta h Q^{R}(T)} \exp(-\beta V_{MEP}(s))$$

In this equation, s is the location of the generalized transition state on the IRC; σ is the symmetry factor accounting for the

S1089-5639(97)02959-9 CCC: $15.00
Published on Web 01/23/1998

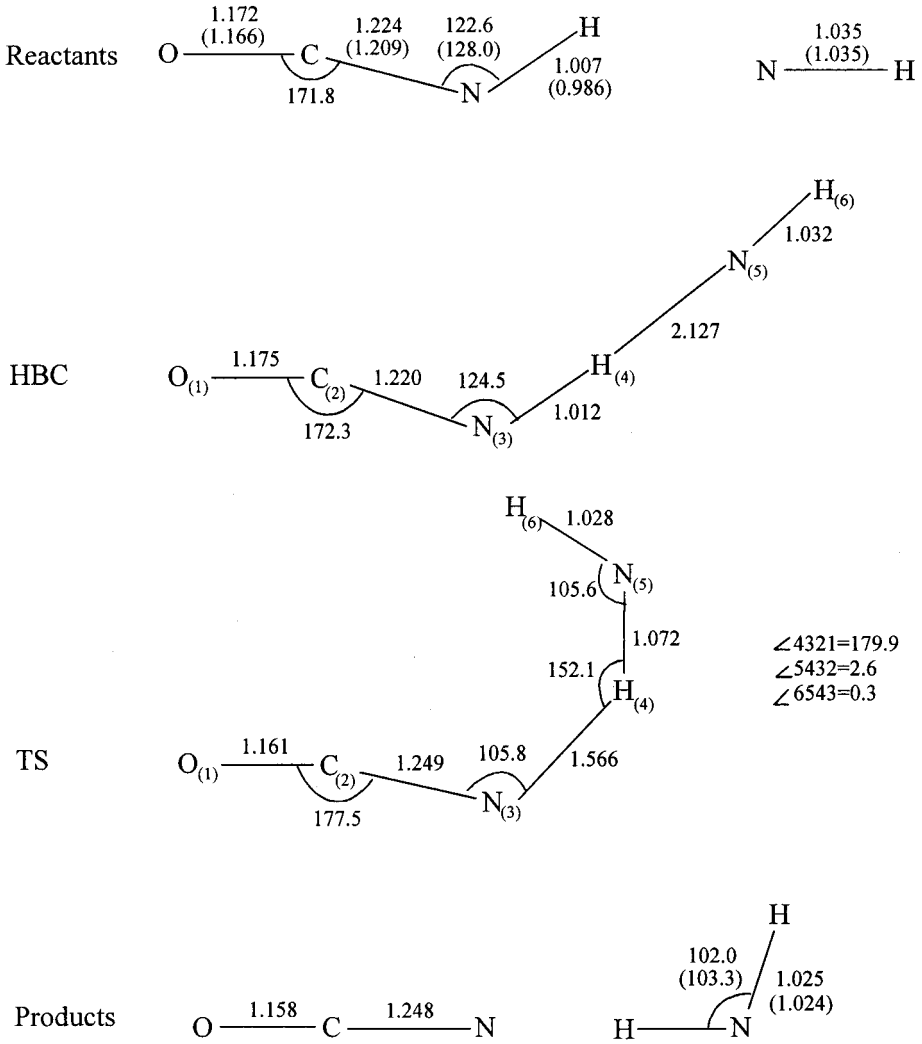

Figure 1. Geometric parameters (in Å and deg) of the reactants, products, hydrogen-bonded complex (HBC), and transition state (TS) at the UMP2/6-311G** level. The numbers in parentheses are the experimental values (ref 17).

possibility of two or more symmetry-related reaction paths; β equals $(k_B T)^{-1}$ where k_B is Boltzmann's constant, h is Planck's constant; $Q^R(T)$ is the reactant's partition function per unit volume, excluding symmetry numbers for rotation; $V_{MEP}(s)$ is the classical energy along the MEP overall zero of energy at the reactants; $Q^{GT}(T,s)$ is the partition function of generalized transition state at s with the local zero of energy at $V_{MEP}(s)$ and with all rotational symmetry numbers set to unity. For $s = 0$, this equation becomes the expression of conventional transition-state theory rate constant ($k^{\ddagger}$).

For the tunneling effect correction, a semiclassical transmission coefficient $\kappa^{CVT/MEPSAG}$ has been used, in which the SAG represents a semiclassical adiabatic ground-state method. Therefore, the variational transition-state rate constant becomes

$$k^{CVT/MEPSAG}(T) = \kappa^{CVT/MEPSAG}(T)\ k^{CVT}(T)$$

The $\kappa^{CVT/MEPSAG}(T)$ may be expressed as

$$\kappa^{CVT/MEPSAG}(T) = \beta \exp(\beta V_a^G(s_*^{CVT}(T))) \int_0^\infty P^{SAG}(E) \times \exp(-\beta E)\, dE$$

Here, E is the total energy of the system relative to reactants; $P^{SAG}(E)$ is the one-dimensional transmission probability that corresponds to passing through the adiabatic ground-state potential energy curve $V_a^G(s)$; s_*^{CVT} is the temperature-dependent value of s at which k^{GT} has a minimum, i.e., location of the CVT transition state; $V_a^G(s)$ is the vibrationally adiabatic ground-state potential curve defined by $V_a^G(s) = V_{MEP}(s) + \epsilon_{int}^G(s)$, where $\epsilon_{int}^G(s)$ denotes the zero-point energy in vibrational modes transverse to the IRC.

To further consider the effect of the curvature of reaction path, $\kappa^{CVT/MEPSAG}(T)$ is corrected by a small-curvature (SC) approximation, which uses an effective mass for reaction coordinate motion, and then is expressed as $\kappa^{CVT/SCSAG}(T)$. Therefore, the variational transition-state rate constant is as follows:

$$k^{CVT/SCSAG}(T) = \kappa^{CVT/SCSAG}(T)\ k^{CVT}(T)$$

The POLYRATE program[16] was employed to the calculations for theoretical rate constants.

Results and Discussion

A. Stationary Points. The geometric parameters of all the stationary points optimized at the UMP2/6-311G** level of theory are shown in Figure 1. For the reactants and products, the optimized geometric parameters are in good agreement with the experimental values. From this figure, it can be seen that the hydrogen abstraction reaction between HNCO and NH proceeds via a hydrogen-bonded complex (HBC) and a transition state (TS):

TABLE 1: Harmonic Vibrational Frequencies (cm^{-1}) of All the Stationary Points

NH	HNCO	HBC	TS	NCO	NH_2
3386.79(3282)[a]	3730.64(3538.25)	3638.23	3484.22	2482.82(1921.30)	3546.35(3301.11)
	2359.84(2268.89)	3432.35	2588.31	1302.63(1272.9)	3447.89(3219.37)
	1305.55(1327)	2363.36	2070.18	627.27	3546.35(3301.11)
	782.30(776.62)	1308.96	1361.31	580.67(535.4)	
	628.21(656.29)	821.17	1286.63		
	558.15(571.35)	644.84	674.98		
		611.19	663.24		
		412.53	619.22		
		197.68	410.39		
		159.09	115.80		
		144.39	62.98		
		52.16	i760.34		

[a] In parentheses, experimental values (ref 18 for NH and ref 19 for HNCO, NCO, and NH_2).

TABLE 2: Total Energies (E) and Relative Energies (ΔE) of All the Stationary Points at the UMP2/6-311G Optimized Geometries**

	E (au)			ΔE (kcal/mol)			ΔE + ZPE[a] (kcal/mol)		
	UMP2	UMP4	UQCI	UMP2	UMP4	UQCI	UMP2	UMP4	UQCI
HNCO	−168.304 30	−168.335 73	−168.328 59						
NH	−55.088 30	−55.107 74	−55.109 18	0	0	0	0	0	0
HBC	−223.400 10	−223.450 61	−223.444 95	−4.71	−4.48	−4.50	−3.30	−3.07	−3.10
TS	−223.344 97	−223.401 79	−223.402 86	29.88	26.15	21.91	30.68	26.95	22.71
NCO	−167.616 30	−167.652 63	−167.652 61						
NH_2	−55.732 65	−55.753 14	−55.754 47	27.39	23.66	19.26	28.45	24.72	20.32

[a] The relative energy corrected by zero-point vibrational energy (ZPE).

$$\text{reactants} \rightarrow \text{HBC} \rightarrow \text{TS} \rightarrow \text{products}$$

The hydrogen-bonded complex (HBC) has a bond distance ($H_{(4)}-N_{(5)}$) of 2.127 Å, and the other bond lengths and bond angles of HBC are very close to those of the reactants (HNCO and NH). In the transition-state structure, the $N_{(3)}-H_{(4)}$ bond length that is broken increases by 55% and the $H_{(4)}-N_{(5)}$ bond length that is formed increases by 4.5% with respect to HNCO and NH_2, respectively. It is obvious that the transition-state structure is like the products. Therefore, the hydrogen abstraction reaction proceeds via a "later" transition state.

Table 1 lists the harmonic vibrational frequencies of the reactants, products, hydrogen-bonded complex, and transition state at the UMP2/6-311G** level of theory. The calculated frequencies of the reactants and products are slightly greater than those of the experimental values. The small geometrical variations between the hydrogen-bonded complex and the reactants cause very little change in the harmonic vibrational frequencies of the complex. The smallest five values of the HBC frequencies correspond to the restricted motions that previously were free rotations and translations of the reactants. The transition state has one and only one imaginary frequency. The eigenvector corresponding to the imaginary vibration mode is associated with the reaction coordinate.

The total energies of the reactants, products, hydrogen-bonded complex, and transition state calculated at three levels of theory are listed in Table 2, together with the energy changes relative to reactants. From this table, one can find that since the energy of HBC with the ZPE correction is about 3 kcal/mol less than that of the reactants, HBC is more stable than the reactants. The heats of reaction with the ZPE correction at the MP2, MP4, and UQCISD(T) levels are 28.45, 24.72, and 20.32 kcal/mol, respectively. The heat of reaction at the UQCISD(T) level is in excellent agreement with the experimental value, 20.50 kcal/mol, which is obtained by the experimental heats of formation (NH, 86 kcal/mol;[20] NH_2, 47.2 kcal/mol;[20] HNCO, −27.90 kcal/mol[21]) and the theoretical heat of formation (NCO, 31.4 kcal/mol[22]).

TABLE 3: Forward and Reverse Reaction Potential Barrier (in kcal/mol)

	reaction potential barrier			reaction potential barrier with ZPE		
	UMP2	UMP4	UQCI	UMP2	UMP4	UQCI
forward	34.59	30.63	26.41	33.98	30.02	25.80
reverse	2.49	2.49	2.65	2.23	2.23	2.39

Table 3 lists the forward and reverse reaction potential energy barriers at the UMP2, UMP4, and UQCISD(T) levels. The forward reaction potential energy barrier with the ZPE correction at the UQCISD(T) level is 25.80 kcal/mol. It is only 1.8 kcal/mol higher than that estimated by Mertens and co-workers.[2] Therefore, the UQCISD(T) result may be considered to be the most reliable. The reverse reaction potential energy barrier at both the UMP2 and the UMP4 levels are the same and are only 0.16 kcal/mol lower than that at the UQCISD(T) level. Because the reverse reaction barrier is far less than the forward reaction barrier, it may be expected that the reverse reaction happens more easily than the forward reaction.

For the triplet ground-state potential energy surface, the correct value of the expectation of s^2 (where s denotes electron spin angular momentum in units of $\hbar$) should be 2.000. Since $\langle s^2 \rangle$s of HBC and TS are 2.016 and 2.077, respectively, the spin contamination for this reaction is not severe. To further illustrate the feasibility of an unrestricted Hartree−Fock single-configuration state, a multiconfiguration self-consistent field (MCSCF) calculation was carried out to optimize the transition state. A complete active space involving six electrons and six orbitals was employed with the 6-311G** basis set. The result shows that the coefficient of the ground-state configuration is 0.970 and those of other configurations are all less than 0.122. Therefore, a single ground-state determinant wave function can describe the characteristic of this reaction accurately.

B. Reaction Path Properties. The reaction path was calculated by the intrinsic reaction coordinate theory at the UMP2/6-311G** level of theory from the transition state to both the asymptotic HBC and product channels. Then, the minimum-energy path was refined with the UQCISD(T) method to obtain

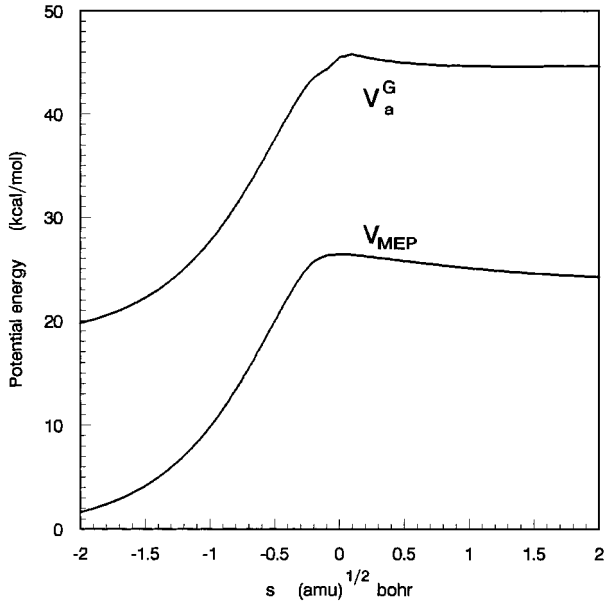

Figure 2. Classical potential energy curve (V_{MEP}) and vibrationally adiabatic ground-state potential energy curve (V_a^G) as a function of s (amu)$^{1/2}$ a_0.

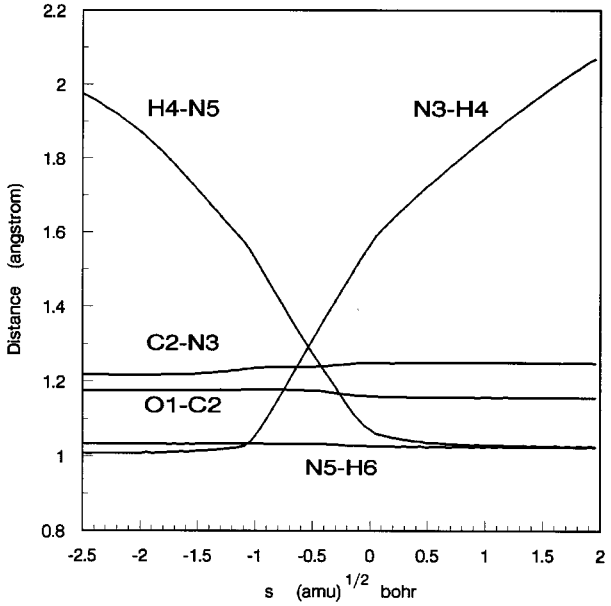

Figure 3. Changes of the main bond lengths (in Å) as a function of s (amu)$^{1/2}$ a_0.

a more reliable potential energy curve. The classical potential energy curve (V_{MEP}) and the vibrationally adiabatic ground-state potential energy curve (V_a^G) along the IRC are plotted in Figure 2. There are the different positions of maximum values for the two potential energy curves. The maximum of V_a^G is located at about $s = 0.1$ (amu)$^{1/2}$ a_0. Perhaps this has influence on the variational effect of the reaction path.

Figure 3 describes the bond length changes of the reaction system along the IRC. It is obviously seen that the dominant reaction coordinates, $N_{(3)}-H_{(4)}$ and $H_{(4)}-N_{(5)}$, change strongly in the course of the hydrogen abstraction reaction, and the others have very small changes. The $N_{(3)}-H_{(4)}$ bond length, which is broken, elongates linearly after about $s = -1.1$ (amu)$^{1/2}$ a_0 along the IRC, and this bond goes to separation as the reaction proceeds. The $H_{(4)}-N_{(5)}$ distance rapidly shortens from $s = -\infty$ and arrives at the bond length of NH_2 at about $s = 0.2$ (amu)$^{1/2}$ a_0. It can be seen that the geometric change mainly

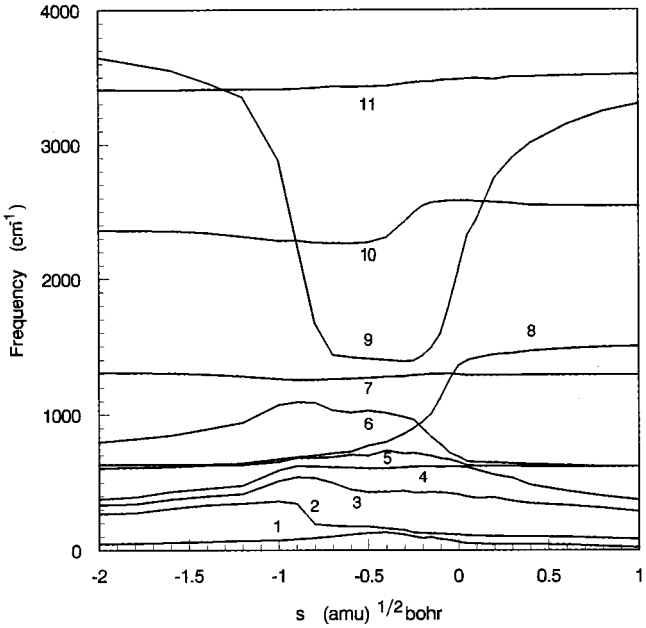

Figure 4. Generalized normal-mode vibrational frequencies as a function of s (amu)$^{1/2}$ a_0.

takes place in the region from about $s = -1.1$ (amu)$^{1/2}$ a_0 to 0.2 (amu)$^{1/2}$ a_0 and the reactive region is ahead of the transition state.

The changes of the generalized normal-mode vibrational frequencies along the IRC are drawn in Figure 4. In the negative limit of s ($s = -\infty$), the generalized normal-mode frequencies correspond to that of HBC, and, in the positive limit of s ($s = +\infty$), the frequencies are associated with the products. The four vibrational modes of the lowest frequencies appear only near the transition state, and their frequencies tend to zero in the directions of the reactants and the products. Modes 5, 6, 7, 10 go to the NCO vibrational frequencies as the reaction proceeds. These frequency curves have no great fluctuation because there is only small variation for the structure of the three atoms in the proceeding of the hydrogen abstraction reaction. The frequency curve of mode 11 is almost unchanged along the IRC since this mode mainly contains the $N_{(5)}-H_{(6)}$ stretching vibration. Mode 8 corresponds to the bending vibration of the product NH_2, so its frequency curve rapidly goes up near the transition state and reaches the frequency of the NH_2 bending vibration. The frequency curve of mode 9 has the greatest variation in the course of the reaction because it connects the frequency of the $N_{(3)}-H_{(4)}$ stretching vibration of HNCO with the frequency of the $H_{(4)}-N_{(5)}$ stretching vibration of NH_2. Therefore, mode 9 can be referred to as the "reactive mode" in the hydrogen abstraction reaction. From Figure 4, it can be seen that mode 9 undergoes a deep frequency valley of about 2000 cm^{-1} and the width of the frequency valley is the region from about $s = -1.2$ (amu)$^{1/2}$ a_0 to 0.4 (amu)$^{1/2}$ a_0 on the IRC. The position of the frequency valley looks like the region of the main geometric changes.

By analyzing the change of the displacement vector of mode 9 along the IRC, we found the vibrational transformation from the $N_{(3)}-H_{(4)}$ stretching vibration to the $H_{(4)}-N_{(5)}$ stretching vibration. Before the point of about $s = -0.7$ (amu)$^{1/2}$ a_0, there is only the $N_{(3)}-H_{(4)}$ stretching vibration, and, after the point of about $s = -0.3$ (amu)$^{1/2}$ a_0, the $H_{(4)}-N_{(5)}$ stretching vibration exists only. Between -0.7 (amu)$^{1/2}$ a_0 and -0.3 (amu)$^{1/2}$ a_0 on the IRC, the approximate symmetric stretching vibration appears in the $N_{(3)}-H_{(4)}-N_{(5)}$ structure. Namely, in this interval the

TABLE 4: Forward Reaction Rate Constants (cm^3 mol^{-1} s^{-1}) for the Temperature Range 1000−3000 K

	T (K)										
	1000	1200	1400	1600	1800	2000	2200	2400	2600	2800	3000
						UMP2/6-311G**					
$k^{\ddagger}$	1.28×10^8	3.35×10^9	3.68×10^{10}	2.33×10^{11}	1.01×10^{12}	3.39×10^{12}	9.32×10^{12}	2.21×10^{13}	4.66×10^{13}	8.96×10^{13}	1.60×10^{14}
k^{CVT}	5.01×10^6	1.09×10^8	1.02×10^9	5.60×10^9	2.14×10^{10}	6.36×10^{10}	1.57×10^{11}	3.37×10^{11}	6.49×10^{11}	1.15×10^{12}	1.89×10^{12}
$k^{CVT/MEPSAG}$	5.33×10^6	1.14×10^8	1.05×10^9	5.72×10^9	2.18×10^{10}	6.45×10^{10}	1.59×10^{11}	3.40×10^{11}	6.54×10^{11}	1.15×10^{12}	1.90×10^{12}
$k^{CVT/SCSAG}$	5.37×10^6	1.15×10^8	1.06×10^9	5.74×10^9	2.18×10^{10}	6.46×10^{10}	1.59×10^{11}	3.40×10^{11}	6.54×10^{11}	1.15×10^{12}	1.90×10^{12}
						UQCISD(T)/6-311G**					
$k^{\ddagger}$	7.89×10^9	1.03×10^{11}	6.95×10^{11}	3.05×10^{12}	9.97×10^{12}	2.65×10^{13}	6.05×10^{13}	1.23×10^{14}	2.27×10^{14}	3.89×10^{14}	6.30×10^{14}
k^{CVT}	3.02×10^8	3.34×10^9	1.91×10^{10}	7.25×10^{10}	2.09×10^{11}	4.94×10^{11}	1.01×10^{12}	1.86×10^{12}	3.14×10^{12}	4.96×10^{12}	7.41×10^{12}
$k^{CVT/MEPSAG}$	3.31×10^8	3.55×10^9	2.00×10^{10}	7.50×10^{10}	2.14×10^{11}	5.04×10^{11}	1.03×10^{12}	1.89×10^{12}	3.18×10^{12}	5.01×10^{12}	7.47×10^{12}
$k^{CVT/SCSAG}$	3.37×10^8	3.59×10^9	2.02×10^{10}	7.56×10^{10}	2.15×10^{11}	5.06×10^{11}	1.03×10^{12}	1.89×10^{12}	3.18×10^{12}	5.02×10^{12}	7.49×10^{12}
exptl[2]	1.23×10^8	9.06×10^8	3.78×10^9	1.10×10^{10}	2.54×10^{10}	4.95×10^{10}	8.53×10^{10}	1.34×10^{11}	1.97×10^{11}	2.75×10^{11}	3.65×10^{11}

TABLE 5: Reverse Reaction Rate Constants (cm^3 mol^{-1} s^{-1}) for the Temperature Range 1000−3000 K

	T (K)										
	1000	1200	1400	1600	1800	2000	2200	2400	2600	2800	3000
						UMP2/6-311G**					
$k^{\ddagger}$	7.29×10^{15}	1.07×10^{16}	1.53×10^{16}	2.09×10^{16}	2.78×10^{16}	3.61×10^{16}	4.58×10^{16}	5.72×10^{16}	7.03×10^{16}	8.52×10^{16}	1.02×10^{17}
k^{CVT}	2.86×10^{14}	3.51×10^{14}	4.23×10^{14}	5.01×10^{14}	5.86×10^{14}	6.76×10^{14}	7.72×10^{14}	8.73×10^{14}	9.79×10^{14}	1.09×10^{15}	1.20×10^{15}
$k^{CVT/MEPSAG}$	3.04×10^{14}	3.66×10^{14}	4.35×10^{14}	5.13×10^{14}	5.96×10^{14}	6.85×10^{14}	7.80×10^{14}	8.81×10^{14}	9.86×10^{14}	1.10×10^{15}	1.21×10^{15}
$k^{CVT/SCSAG}$	3.06×10^{14}	3.68×10^{14}	4.38×10^{14}	5.14×10^{14}	5.97×10^{14}	6.86×10^{14}	7.82×10^{14}	8.82×10^{14}	9.87×10^{14}	1.10×10^{15}	1.21×10^{15}
						UQCISD(T)/6-311G**					
$k^{\ddagger}$	6.72×10^{15}	1.01×10^{16}	1.44×10^{16}	1.98×10^{16}	2.65×10^{16}	3.46×10^{16}	4.41×10^{16}	5.53×10^{16}	6.81×10^{16}	8.27×10^{16}	9.91×10^{17}
k^{CVT}	2.60×10^{14}	3.25×10^{14}	3.95×10^{14}	4.73×10^{14}	5.53×10^{14}	6.45×10^{14}	7.40×10^{14}	8.40×10^{14}	9.49×10^{14}	1.05×10^{15}	1.17×10^{15}
$k^{CVT/MEPSAG}$	2.85×10^{14}	3.45×10^{14}	4.13×10^{14}	4.89×10^{14}	5.71×10^{14}	6.58×10^{14}	7.52×10^{14}	8.51×10^{14}	9.55×10^{14}	1.06×10^{15}	1.18×10^{15}
$k^{CVT/SCSAG}$	2.90×10^{14}	3.50×10^{14}	4.17×10^{14}	4.92×10^{14}	5.74×10^{14}	6.62×10^{14}	7.55×10^{14}	8.53×10^{14}	9.57×10^{14}	1.07×10^{15}	1.18×10^{15}

transformation of the vibrational vector of mode 9 from the $N_{(3)}-H_{(4)}$ stretching vibration to the $H_{(4)}-N_{(5)}$ stretching vibration is finished. Therefore, this interval may be a demarcation dividing the reactant side from product side. The hydrogen abstraction reaction not only passes over the potential energy barrier but also must undergo the transformation of the vibrational vector of mode 9.

C. Rate Constant Calculation. Using the reaction path Hamiltonian parameters,[23,24] the potential energy curve, and the first and second energy derivatives, we obtained the forward and the reverse reaction rate constants for the temperature range 1000−3000 K by the conventional transition-state theory and the variational transition-state theory. Tables 4 and 5 list the forward and reverse reaction rate constants, respectively, calculated at the UMP2 and UQCISD(T) levels of theory. From these two tables, one can find that the variational effect affects strongly the rate constant calculation. The rate constants of the variational transition state theory (k^{CVT}) at the temperatures 1000, 2000, and 3000 K are about 25, 53, and 84 times less than the rate constants of the conventional transition state theory ($k^{\ddagger}$), respectively. Besides, we can find that the tunneling and curvature effects have a very small influence on the reaction rate constants.

For the forward reaction, the CVT/SCSAG rate constants at the UMP2 level are less than the experimental rate constants at $T < 2000$ K and greater than the experimental rate constants at $T > 2000$ K. At the UQCISD(T) level, the CVT/SCSAG rate constants are about 2.7, 10.2, and 20.5 times the experimental rate constants at the temperatures 1000, 2000, and 3000 K, respectively. Apparently, the UQCISD(T) level gives the upper limit of the rate constants. The comparison of the forward reaction rate constants are plotted in Figure 5.

In addition, for the reverse reaction the theoretical rate constants at the UMP2 level are slightly greater than those at the UQCISD(T) level. The reverse reaction rate constants are located between the 14th and 15th power of 10, and the reverse reaction rate constants are at least an order of magnitude greater than the forward reaction rate constants. Therefore, the reverse reaction may happen more easily than the forward reaction.

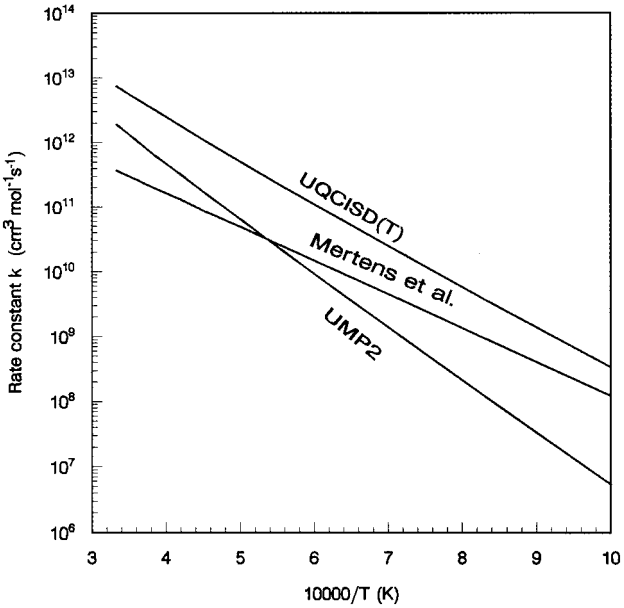

Figure 5. Arrhenius plot of the forward reaction rate constants *k* (cm^3 mol^{-1} s^{-1}) along the reciprocal of the temperature (K) over the temperature range 1000−3000 K.

Conclusion

In this work, the hydrogen abstraction reaction between HNCO and NH has been carefully investigated. A few conclusions from the above discussion are as follows:

(1) The two stationary points are first located at the UMP2/6-311G** level of theory. The first one is a hydrogen-bonded complex (HBC) close to the reactants (HNCO and NH). The hydrogen-bonded complex is 3.10 kcal/mol more stable than the reactants at the UQCISD(T)/6-311G** level of theory. The

second is the transition state of the hydrogen abstraction reaction path, which has energy 22.71 kcal/mol above the reactants at the UQCISD(T)/6-311G** level. Thus, we obtained that the forward and reverse reaction potential energy barriers are 25.80 and 2.39 kcal/mol, respectively. Because the heat of reaction is 20.32 kcal/mol at the UQCISD(T)/6-311G** level, the hydrogen abstraction reaction is very endothermic.

(2) By analyzing the geometric change of the hydrogen abstraction reaction along the IRC, we have found that the reactive region of the bond breaking and the bond forming is about from $s = -1.1$ to 0.2 $(\text{amu})^{1/2}$ a_0. The main geometric change takes place ahead of the transition state. By analyzing the changes of the generalized normal-mode vibrational frequencies along the IRC, we have also found mode 9 describes the processing of the hydrogen abstraction reaction. This is a "reactive mode".

(3) The forward and the reverse reaction rate constants for the temperature range 1000−3000 K were obtained by the variational transition-state theory at the UQCISD(T) level of theory. The theoretical rate constants of the forward reaction are about 2.7, 10.2, and 20.5 times the experimental rate constants at the temperatures 1000, 2000, and 3000 K, respectively. The reverse reaction rate constants are at least an order of magnitude greater than the forward reaction rate constants. In addition, we have found that the tunneling and curvature effects have a very small influence on the reaction rate constants.

Acknowledgment. This work was supported by the National Natural Science Foundation of China and by the National Laboratory of Theoretical and Computational Chemistry of Jilin University.

References and Notes

(1) Perry, R. A.; Siebers, D. L. *Nature* **1986**, *324*, 657

(2) Miller, J. A.; Bowman, C. T. *Prog. Energy Combust. Sci.* **1989**, *15*, 287.

(3) Mertens, J. D.; Kohse-Honghans, K.; Hanson, R. K.; Bowman, C. T. *Int. J. Chem. Kinet.* **1991**, *23*, 655.

(4) Frisch, M. J.; Trucks, G. W.; Head-Gordon, M.; Gill, P. M. W.; Wong, M. W.; Foresman, J. B.; Johnson, B. G.; Schlegel, H. B.; Robb, M. A.; Replogle, E. S.; Gomperts, R.; Andres, J. L.; Raghavachari, K.; Binkley, J. S.; Gonzalez, C.; Martin, R. L.; Fox, D. J.; Defrees, D. J.; Stewart, J. J. P.; Pople, J. A. *Gaussian 92;* Gaussian, Inc.: Pittsburgh, PA, 1992.

(5) Hehre, W. J.; Radom, L.; Schleyer, P. V. R.; Pople, J. A. *Ab Initio Molecular Orbital Theory*; Wiley: New York, 1986.

(6) Pople, J. A.; Binkley, J. S.; Seeger, R. *Int. J. Quantum Chem. Symp.* **1976**, *10*, 1.

(7) Pople, J. A.; Head-Gordon, M.; Raghavachari, K. *J. Chem. Phys.* **1987**, *87*, 5968.

(8) Fukui, K. *J. Phys. Chem.* **1970**, *74*, 4161.

(9) Gonzalez, C.; Schlegel, H. B. *J. Phys. Chem.* **1989**, *90*, 2154.

(10) Gonzalez, C.; Schlegel, H. B. *J. Phys. Chem.* **1990,** *94*, 5523.

(11) Keck, J. C. *J. Chem. Phys.* **1960**, *32*, 1035.

(12) Truhlar, D. G.; Garrett, B. C. *Acc. Chem. Res* **1980**, *13*, 440.

(13) Garrett, B. C.; Truhlar, D. G.; Grev, R. S.; Magnuson, A. W. *J. Phys. Chem.* **1980**, *84*, 1730.

(14) Truhlar, D. G.; Isaacson, A. D.; Garrett, B. C. In *Theory of Chemical Reaction Dynamics*; Baer, M., Ed.; CRC Press: Boca Raton, FL, 1985; p 65.

(15) Baldridge, K. M.; Gordon, M. S.; Steckler, R.; Truhlar, D. G. *J. Phys. Chem.* **1989**, *93*, 5107.

(16) Isaacson, A. D.; Truhlar, D. G.; Rai, S. N.; Steckler, R.; Hancock, G. C. *POLYRATE Version 1.0*; University of Minnesota: Minneapolis, MN, 1987.

(17) Harmony, M. D.; Laurie, V. W.; Kuczkowski, R. L.; Schwendeman, R. H.; Ramsay, D. A.; Lovas, F. J.; Lafferty, W. J.; Maki, A. G. *J. Phys. Chem. Ref. Data* **1979**, *8*, 619.

(18) Huber, K. P.; Herzberg, G. *Molecular Spectra and Molecular Structure (IV). Constants of Diatomic Molecules*; Van Nostrand Reinhold: New York, 1979.

(19) Jacox, M. E. *J. Phys. Chem. Ref. Data* **1990**, *19*, 1387.

(20) Kerr, J. A.; Parsonage, M. J.; Trotman-Dickenson, A. F. In *Handbook of Chemstry and Physics*, 55th *ed.;* West, Robert, Ed.; CRC Press: Boca Raton, FL, 1974; p F-219.

(21) *Lange's Handbook of Chemistry*, 13th ed.; Dean, J. A., Ed.; McGraw-Hill Book Company: New York, 1985.

(22) East, A. L. L.; Allen, W. D. *J. Chem. Phys.* **1993**, *99*, 4638.

(23) Miller, W. H.; Handy, N. C.; Adams, J. C. *J. Chem. Phys.* **1980**, *72*, 99.

(24) Miller, W. H. In *Potential Energy Surface and Dynamics Calculations*; Truhlar, D. G., Ed; Plenm Press: New York, 1981; p 265.